

Electron energization during merging of self-magnetized, high-beta, laser-produced plasmas

G. Fiksel^{1,†}, W. Fox^{2,3}, M.J. Rosenberg⁴, D.B. Schaeffer³, J. Matteucci² and A. Bhattacharjee^{2,3}

¹Center for Ultrafast Optical Science, University of Michigan, Ann Arbor, MI, USA

²Princeton Plasma Physics Laboratory, Princeton, NJ, USA

³Department of Astrophysical Sciences, Princeton University, Princeton, NJ, USA

⁴Laboratory for Laser Energetics, University of Rochester, Rochester, NY, USA

(Received 22 February 2021; revised 4 July 2021; accepted 6 July 2021)

Electron energization during merging of magnetized plasmas is studied using the OMEGA and OMEGA EP laser facilities by colliding two plasma plumes, each containing a Biermann-battery self-generated magnetic field. Two neighbouring plasma plumes are produced by intense laser beams, and the anti-parallel Biermann fields merge and reconnect in the process of the plumes' expansion and collision. To isolate the merging as an acceleration source, the electron energy spectra obtained from two-plume collision shots are compared with the spectra from single-plume shots. Single-plume shots exhibit an energized electron tail with energies up to ~ 250 keV. The electrons in merging experiments are additionally accelerated by ~ 50 – 100 keV compared to single-plume shots.

Key words: astrophysical plasmas

1. Introduction

Energetic charged particles observed in solar and Earth's magnetosphere plasmas (Lin & Forbes 2000; Bhattacharjee 2004; Birn *et al.* 2012; Fu *et al.* 2013; Chen *et al.* 2020) and in laboratory plasmas (Yamada *et al.* 1994; Hsu *et al.* 2001; Fiksel *et al.* 2009; Fox *et al.* 2010; Yamasaki *et al.* 2015; Tanabe *et al.* 2017) are frequently associated with magnetic reconnection (Parker 1963; Priest & Forbes 2000), a process of changing the topology of magnetic fields and thereby allowing an explosive release of stored magnetic energy.

Magnetic reconnection in high-energy-density laser-produced plasmas has been extensively studied (Nilson *et al.* 2006, 2008; Li *et al.* 2007; Dong *et al.* 2012; Fiksel *et al.* 2014; Rosenberg *et al.* 2015*a,b*; Fox *et al.* 2020) and plasma heating and the presence of super-thermal energetic electrons have been documented (Zhong *et al.* 2010, 2016). Nevertheless, although high-energy electrons have been detected, the mechanism of their acceleration still remains poorly understood. Moreover, contributions from alternative

[†] Email address for correspondence: gfiksel@umich.edu

acceleration mechanisms, such as laser–plasma interaction (LPI) (Kruer 1988; Regan *et al.* 1999), formation of collisionless shocks (Schaeffer *et al.* 2017), tearing (plasmoid) and Weibel instabilities (Bhattacharjee 2004; Drake, Swisdak & Fermo 2012; Hoshino 2012; Fox *et al.* 2013, 2017; Huntington *et al.* 2015) and the betatron effect (Somov *et al.* 2003; Chen *et al.* 2020), are not ruled out and, as such, the role of reconnection in the acceleration is only conjectured.

We report on experiments conducted using the OMEGA (Boehly 1977) and OMEGA EP (Waxer *et al.* 2005) laser facilities, which provide a conclusive observation of particle energization in experiments where collision, merging and reconnection of two magnetized plasmas take place.

To initiate a collision, two neighbouring plasma plumes are produced by intense laser beams, and the magnetic fields, self-generated via the Biermann battery effect (Biermann 1950), merge and reconnect in the process of the plumes' expansion. To characterize the energization, the energy distribution of the electrons escaping the plasmas is measured. To isolate the merging and/or reconnection as an acceleration source, the electron energy spectra obtained from two-plume reconnection shots are compared with the spectra from 'null' single-plume shots.

One important observation is that even in experiments with a single plasma plume, an energized population with energies up to ~ 250 keV and an equivalent temperature of up to ~ 19 keV can be produced. Observing the single-plume spectra is important because they presumably play a role of 'input' to any energization process which occurs during the merging. We also observe that in experiments with two merging plasma plumes, the electrons are additionally accelerated by ~ 50 – 100 keV compared with single-plume shots. This additional energization is significantly beyond the statistical variation between the single- and two-beam experiments, and is confirmed in experiments with both OMEGA and OMEGA EP.

In this paper, we consider several possible energization mechanisms, and find that the additional energization is much larger than could be expected from mechanisms typically associated with reconnection, such as acceleration by the electric field induced in the current sheet or the first-order Fermi acceleration, a process of energy gain via consecutive reflections from two approaching magnetic fields. Another general and important observation is that careful comparison of two-plume merging with single plume is required to confirm the effect of energization. These comparison tests, to our knowledge, have not previously been reported.

The paper is organized as follows. Section 2 describes the experimental set-up and diagnostics. Results of the electron energization are presented in § 3. These results and also several mechanisms of electron energization are discussed in § 4. Section 5 presents justifications of the various plasma parameters used throughout the paper. The results and conclusions are summarized in § 6.

2. Experimental set-up and diagnostics

The experiments were conducted using the OMEGA and OMEGA EP laser facilities with a typical experimental set-up shown in figure 1. A thin plastic (CH) target with a size of 3×5 mm² is driven by one or two 351 nm laser beams, each focused on a spot with a diameter of 750 μ m. The target thickness was 5 μ m for experiments on OMEGA and 25 μ m for experiments on EP.

Each beam has an energy of 200 J for EP and 225 J for OMEGA and a duration of 0.5 ns, which corresponds to a beam power of 0.4–0.45 TW and a nominal on-target laser intensity of 0.9 – 1×10^{14} W cm⁻². The choice of the beam energy and duration was motivated by trying to reduce the effect of electron energization by LPI, such as stimulated

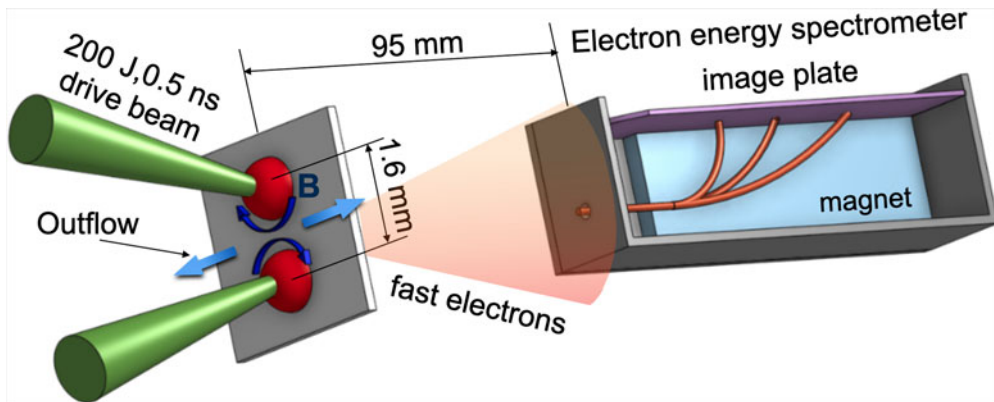


FIGURE 1. Experimental set-up. A plastic (CH) target is driven by one or two nm laser beams focused on a spot with a diameter of $750\ \mu\text{m}$. Each beam has an energy of 200 J and a duration of 0.5 ns. The fast electrons are analysed by a magnetic energy spectrometer placed 95 mm from the target. The electrons entering the spectrometer are dispersed by a permanent magnetic field of 450 G and registered by an image plate placed on top of the magnets.

Raman scattering or two-plasmon decay instability. In general (Rosenberg *et al.* 2020; Solodov *et al.* 2020), LPI intensity and hence electron acceleration increase with the laser beam intensity and duration. For the experiments, a low beam power and a short duration were chosen to minimize this effect.

Two types of shots were investigated: two-plume merging shots and single-plume non-merging shots. For merging shots, two beams focused 1.6 mm apart produce two plasma plumes with anti-parallel self-generated Biermann magnetic fields that merge and reconnect in the process of the plumes' expansion. For non-merging, or 'null', shots only a single beam was used.

The fast electrons were analysed by a magnetic energy spectrometer (Habara *et al.* 2019) placed 95 mm from the target. The majority of the data were obtained with the spectrometer aligned to detect the electrons streaming along the so-called X-line, that is, the line normal to the reconnection current sheet and along which the oppositely directed magnetic fields cancel each other and thus only weakly affect the electron trajectories. In addition, this alignment results in the spectrometer's line of view being aligned with the reconnection-induced electric field, which could be directly related to the electron acceleration. The position of the analyser shown in figure 1 corresponds to the electrons being accelerated by the reconnection-induced electric field. We also show results with the analyser viewing the front face of the target, the direction in which the electrons are expected to be decelerated by the field. Finally, we show results with the analyser aligned parallel to the current sheet, along the 'outflow' direction.

The electrons enter the spectrometer through a 0.7 mm pinhole collimator and are dispersed by a permanent magnetic field of 450 G. The magnetic dispersion was calculated with the COMSOL Multiphysics package using the experimentally measured magnetic field. The dispersion energy range of the spectrometer is from 0.02 to 4 MeV. The dispersed intensity of the electron flux is registered by a Fuji BAS-TR image plate (Miyahara *et al.* 1986; Gales & Bentley 2004) placed on top of the magnets. Image plates are widely used for detection of charged particles and ionizing radiation due to their high sensitivity and linearity over a large energy range. A specific advantage of using the TR type for our purpose is that it does not have a protective mylar film covering the

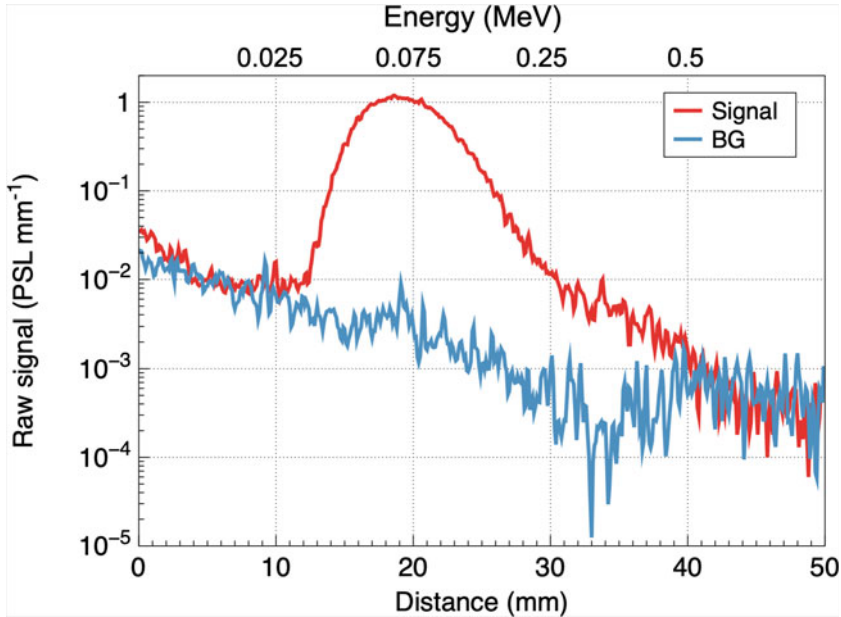


FIGURE 2. A typical plot of PSL (red curve) versus distance along the image plate. The background (BG; blue curve) is caused by scattered X-rays and is subtracted from the total signal for analysis.

photostimulable phosphor layer, thus extending its low-energy range. Since the image plate response is time-integrated, no temporal information is available.

A typical plot of the image plate photostimulated luminescence (PSL) signal integrated across the image plate versus the distance along the image plate is shown in figure 2. Besides the luminescence from the dispersed electrons, there is a contribution from scattered X-rays that is shown in blue and is measured along the part of the image plate not exposed to the electrons. For spectral analysis, the background is subtracted from the total signal. The background level was dependent on the type of shot, i.e. merging or ‘null’, as well as varying from shot to shot.

After scanning the exposed image plate, the PSL profile $d(PSL)/dl$ (in units of $PSL\ mm^{-1}$) is converted to the electron energy spectra dN/dE according to

$$\frac{dN}{dE} = \frac{d(PSL)}{dl} \left(\frac{dE}{dl} \right)^{-1} \left(\frac{d(PSL)}{dN} \right)^{-1}, \quad (2.1)$$

where dE/dl is the spectrometer dispersion and $d(PSL)/dN$ is the image plate sensitivity per electron (Bonnet *et al.* 2013).

3. Electron energization

The energy spectra for merging and non-merging shots measured using OMEGA EP in the direction of X-line acceleration, that is, anti-parallel to the reconnection electric field, are shown in figure 3, where we compare a set of two merging shots with a set of four single-beam ‘null’ shots. Each curve represents the spectra normalized over the number of beams in each shot and then averaged over the respective set. In this normalization, the total laser energy in each group is identical, and if there is no additional energization from merging, one would predict the spectra would be identical as well. The shot-to-shot

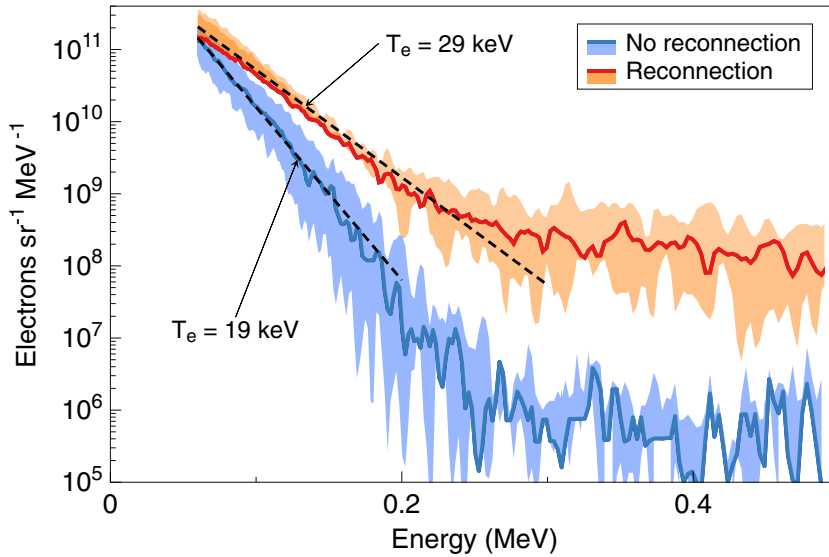


FIGURE 3. Electron energy spectra for merging (red) and non-merging (blue) shots taken using OMEGA EP in the direction of X-line acceleration. The coloured bands represent the standard shot-to-shot deviation.

data scatter is represented by the coloured bands, which span an interval of one standard deviation.

The ‘null’ shot spectrum exhibits an initial exponential slope with an equivalent temperature of 19 keV. The value of the slope is significantly higher than the expected bulk plasma temperature of $T_e = 0.4$ keV. (See § 5 for more details on the plasma density and temperature measurements.) In addition, even though this high-energy tail appears to be Maxwellian, it cannot be supported by classical Coulomb collisions in plasma at such energies. Indeed, estimating an electron mean-free path for a fast electron with an energy E in a plasma with a density $n_e = 1.5 \times 10^{19} \text{ cm}^{-3}$, 1 : 1 C-to-H plasma composition and $\Lambda = 10$, $\lambda[\text{cm}] = 1.25 \times 10^{12} E^2[\text{eV}]/n_e[\text{cm}^{-3}]\Lambda$ (Book 1990), results in $\lambda = 80$ cm for a typical electron energy of $E = 100$ keV. This mean-free path is much larger than a typical plasma size of several millimetres. This observation strongly suggests that other, non-thermal energization mechanisms, for example energization via LPI, are present in the plasma.

The spectrum from the merging shots has an exponential slope that corresponds to an equivalent temperature of 29 keV, an increase by a factor of about 1.5 compared to the ‘null’ shots. Given the spectra normalization procedure described earlier, the fact of the additional electron acceleration strongly suggests that it is a result of the plumes’ collision and/or reconnection. We note here that the plateau part of the spectra at high energies, e.g. higher than 0.4–0.5 MeV in figure 3, represents the background noise from X-ray exposure.

We confirmed the energization effect in separate experiments conducted using OMEGA with a similar experimental set-up employing a similar beam configuration albeit at a 10 % higher beam power (225 J instead of 200 J). In this series of shots we compare one merging shot with two beams with one single-beam ‘null’ shot. Each curve represents the spectra normalized over the respective number of beams. Only one shot for the merging case and one shot for the single beam were taken; therefore, no error bar estimation was possible.

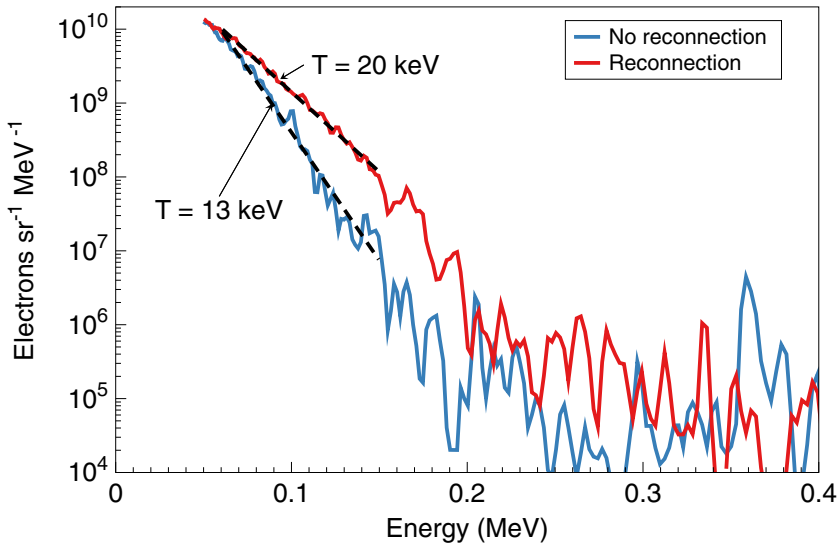


FIGURE 4. Electron energy spectra for merging (red) and non-merging (blue) shots taken using OMEGA in the direction of X-line acceleration.

This series produced similar results – strong electron energization even in the case of a single plasma plume and additional energization for two colliding and merging plumes (figure 4).

We note here that the energy losses from passing through the thin targets are expected to be small. Using the NIST tables (NIST 2021), one can estimate that the range of a 100 keV electron is about 145 μm , much longer than the target thickness, and the energy loss is about 2 keV for OMEGA and 10 keV for EP.

Because of the arrangements of the laser and diagnostic ports of EP, it was not possible to place an analyser viewing the plasma from the direction of X-line deceleration, which is parallel to the reconnection electric field. However, for OMEGA this configuration was possible and the results are shown in figure 5. Relative to the direction of X-line acceleration, the signature of the additional acceleration during the merging of the plumes is very similar, although the signal amplitude is lower. This decrease in the amplitude may agree with the LPI origin of the pre-accelerated electrons, which are predominantly forward-peaked.

Finally, figure 6 shows the energy spectra taken using EP and OMEGA in the outflow direction. The additional acceleration during the merging of the plumes is evident. The ‘outflow’ electrons might be strongly affected by the reconnection magnetic field, so the signal might strongly depend on the angle of the line of sight relative to the target, which in our experiment was very oblique.

To conclude the presentation of the experimental results, we briefly reiterate two major points. First, it has been found that there exists a source of electron energization that is active even in single-plume ‘null’ shots. We speculate that these super-thermal electrons are generated via residual LPI that was not completely eliminated by reducing the laser beam intensity even though its level was below the detection threshold. Most importantly, we confirm additional acceleration found in experiments where two plumes collided and merged, over that observed in single-plume experiments, indicating an effect due to the collision, merging and/or reconnection.

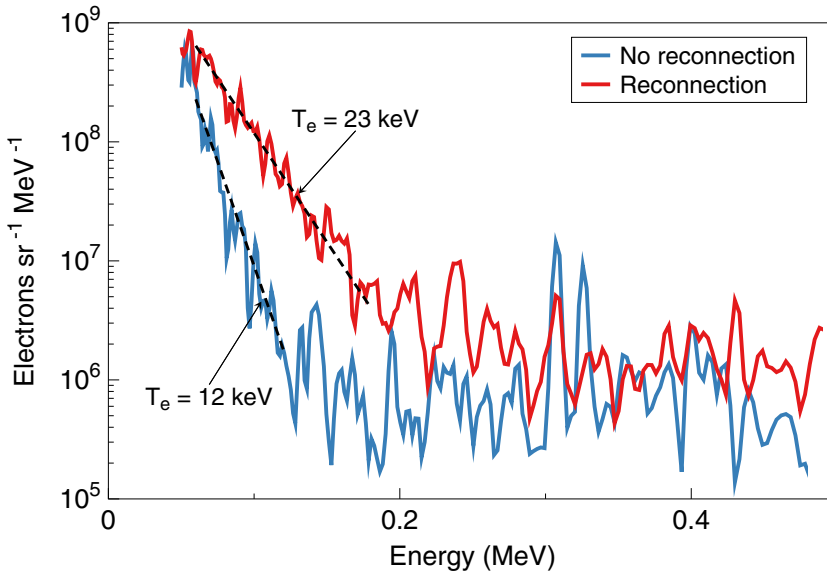


FIGURE 5. Electron energy spectra for merging (red) and non-merging (blue) shots taken using OMEGA in the direction of X-line deceleration.

4. Discussion

Several relevant electron acceleration mechanisms in high-energy-density plasmas have been discussed in the literature, including magnetic reconnection (Zhong *et al.* 2010; Dong *et al.* 2012; Totorica, Abel & Fiuza 2016, 2017; Zhong *et al.* 2016; Fox *et al.* 2017), Fermi acceleration (Drake *et al.* 2012; Hoshino 2012), formation of collisionless shocks (Schaeffer *et al.* 2017), plasma instabilities (Bhattacharjee 2004; Drake *et al.* 2012; Fox *et al.* 2013; Huntington *et al.* 2015; Fox *et al.* 2017) and the betatron effect (Somov *et al.* 2003; Chen *et al.* 2020).

We briefly consider three potential mechanisms for acceleration of energetic super-thermal electrons: (1) X-line acceleration, (2) first-order Fermi acceleration and (3) the betatron effect. We conclude that the two former mechanisms contribute only weakly to acceleration while the latter has all the ingredients for efficient acceleration including a high driving force and a good particle confinement, both necessary for the energization to take place.

4.1. X-line acceleration

The electric field induced by reconnection can in principle accelerate collisionless electrons, especially in the vicinity of X-points where the two reconnecting magnetic fields cancel each other so the electrons become demagnetized and are only weakly affected by the magnetic field. However, simple estimates demonstrate that these effects are expected to be small in our particular case. The energy gain from the electric field \mathcal{E}_z induced in the current sheet is $\Delta E_X = e \int \mathcal{E}_z dz$, where the z axis is directed along the X-line. The electric field can be estimated as $\mathcal{E}_z \sim V_{in} B$, thus

$$\Delta E_X = e V_{in} \int B dz, \quad (4.1)$$

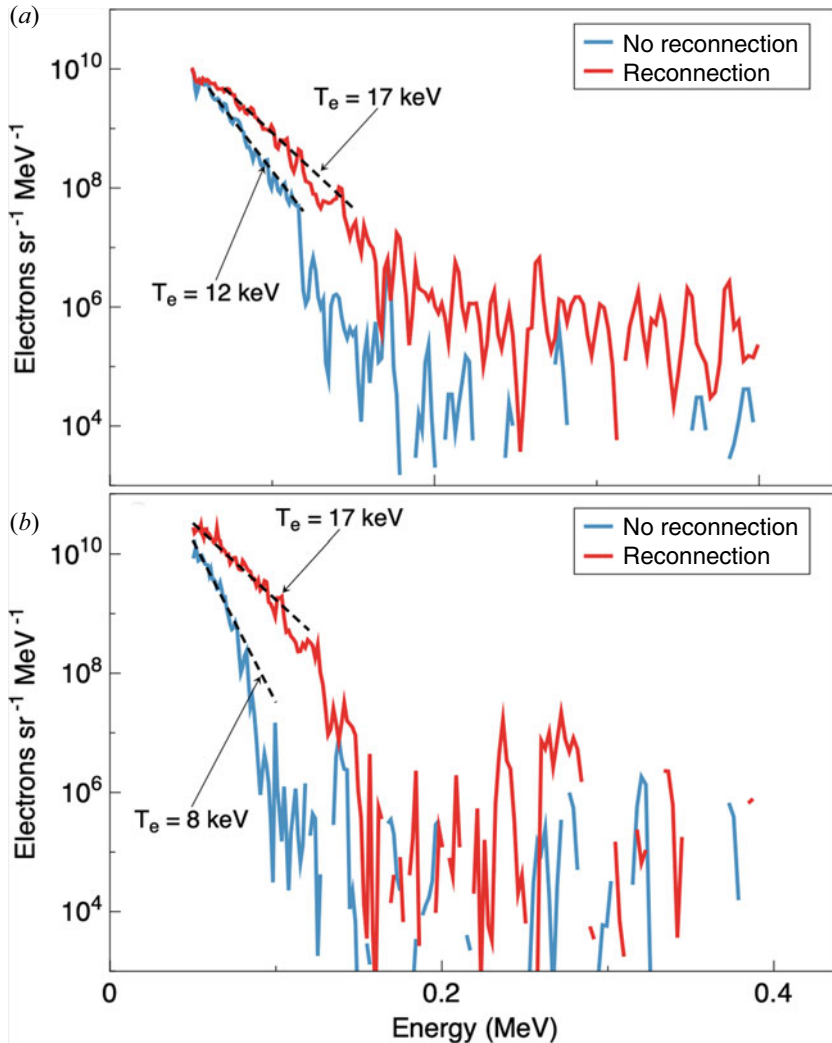


FIGURE 6. Electron energy spectra for merging (red) and non-merging (blue) shots taken using (a) EP and (b) OMEGA in the outflow direction.

where V_{in} is the inflow velocity, B is the plume magnetic field and $\int B dz$ is the magnetic flux per unit of the current sheet length.

From the magnetic field imaging using the fast proton radiography diagnostic under conditions very similar to ours (Petraso *et al.* 2009), the B -integral is $\int B dz \sim 10 \text{ T mm}$ and the flow velocity estimated from the bubble expansion dynamics is $V_{\text{in}} \sim 5 \times 10^5 \text{ m s}^{-1}$. Therefore, the expected energy gain from the reconnection-induced field $\Delta E_X = e \int \mathcal{E}_z dz \sim 5 \text{ keV}$, which is much less than observed. In addition, this mechanism is expected to be weakly dependent on the initial electron energy, whereas the measured spectra clearly indicate that the acceleration favours higher energies. Indeed, given that this high-energy electron tail is collisionless, a constant energy gain across the spectra would have resulted in an energy shift, while the observed change of slope, shown for example in figure 3, indicates that energy gain is approximately proportional to the energy as $\Delta E \approx 0.5E$.

4.2. First-order Fermi acceleration

Previous simulations (Fox *et al.* 2017; Totorica *et al.* 2017) suggested the possibility of the first-order Fermi acceleration process, in which a charged particle is accelerated by bouncing between two approaching magnetic walls. If the relative magnetic wall velocity is much less than the particle velocity, then due to conservation of the adiabatic invariant $\oint p_x dx$ (Landau & Lifshitz 1981), the particle energy is increasing as $E = E_0 l_0^2/l^2$, or the energy gain is

$$\Delta E_F = E_0(l_0^2/l^2 - 1), \quad (4.2)$$

where l is the wall separation and E_0 and l_0 are the initial energy and the initial wall separation.

In general, this mechanism favours the higher energies but in the three-dimensional geometry of the experiment, an electron can escape from the gap between the walls along the unmagnetized direction. The escape time can be estimated as $\tau \sim L/v_e$, where L is a characteristic length and v_e is the electron velocity. Because of the small, ~ 1 mm size of a typical laser plasma experiment, the electron is lost in a very short time. For an electron with an energy of $E_0 = 100$ keV, the escape time over $L = 3$ mm (three times the plasma size) is $\tau \sim 20$ ps. If the two walls, separated initially by $l_0 = 1$ mm, are colliding with a velocity of $V_{in} = 5 \times 10^5$ m s⁻¹, then in that time each wall would move only by $V_{in}\tau \approx 10$ μ m, resulting in a very small compression factor of $l_0^2/l^2 \sim 1.04$, and a corresponding energy gain of only $\Delta E_F = 4$ keV.

4.3. A model of electron acceleration

To evaluate the effects of both acceleration by the reconnection electric field and Fermi acceleration in a cohesive and self-consistent manner, consider a simple toy model of expanding and merging toroidal Biermann fields. Following Kugland *et al.* (2012) consider two merging magnetic toroidal plumes, each with a magnetic field defined by its vector potential:

$$A_z = -\frac{B_0 a}{2} \exp\left(-\frac{x^2 + y^2 + z^2}{a^2}\right), \quad (4.3)$$

where a is the plume radius. The magnetic field is calculated as $\mathbf{B} = \nabla \times \mathbf{A}$ and the electric field as $\mathbf{E} = -\partial \mathbf{A}/\partial t$. Each individual magnetic field, given by (4.3), has closed toroidal flux surfaces typical for a field generated by the Biermann effect, as illustrated in figure 7(a).

Assume that each plume expands according to $a = a_0 + V_{in}t$, where a_0 is the initial plume radius and V_{in} is the expansion velocity. For the particular model, assume $a_0 = 0.5$ mm, $V_{in} = 5 \times 10^5$ m s⁻¹ and select $B_0 = 20$ T, the value that results in the maximum of the line-integrated magnetic field of $\int B dz = 10$ T mm. Figure 7(b) shows a map of the magnetic field across the horizontal cross-section at $t = 0.8$ ns, which is the moment when the plumes start to merge, and figure 7(c) shows the profiles of the magnetic and electric fields and the line integral of the magnetic field at that time.

In order to emulate the conditions of our experiment using this simple model, we follow a group of already pre-energized electrons. To this end, an isotropic source of test electrons with an initial energy of 100 keV is placed between the plumes and their trajectories are traced by solving the relativistic equations of motion with the COMSOL Multiphysics package. The electrons are bouncing between the expanding plumes experiencing a combined action of the direct Fermi effect and the inductive electric field and eventually escape. The trajectories of the electrons, represented in terms of the electron energy, are shown in figure 8. The electrons escaping down the X-line in the direction opposite to

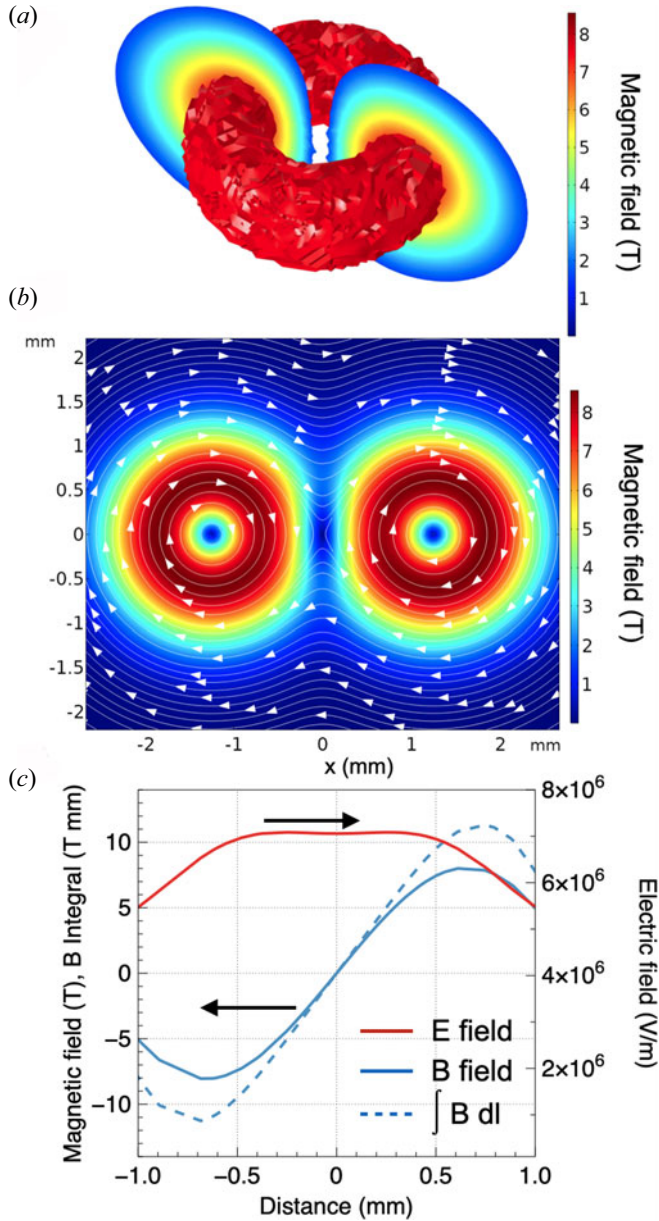


FIGURE 7. Magnetic field topology. (a) A magnetic toroid typical for a field generated by the Biermann effect. The model (b) magnetic field map, and (c) magnetic (blue) and electric (red) fields, and the line integral of the magnetic field (blue, dashed) profiles at $t = 0.8$ ns.

that of the electric field are gaining an energy of up to about 4 keV, in agreement with the previous estimates. To check the effect of the magnetic field, the calculations were repeated at a value of the magnetic field integral of $\int B dz = 25$ T mm. As a result, the energy gain of the escaped electrons increased from 4 to 10 keV, still much lower than observed in the experiment.

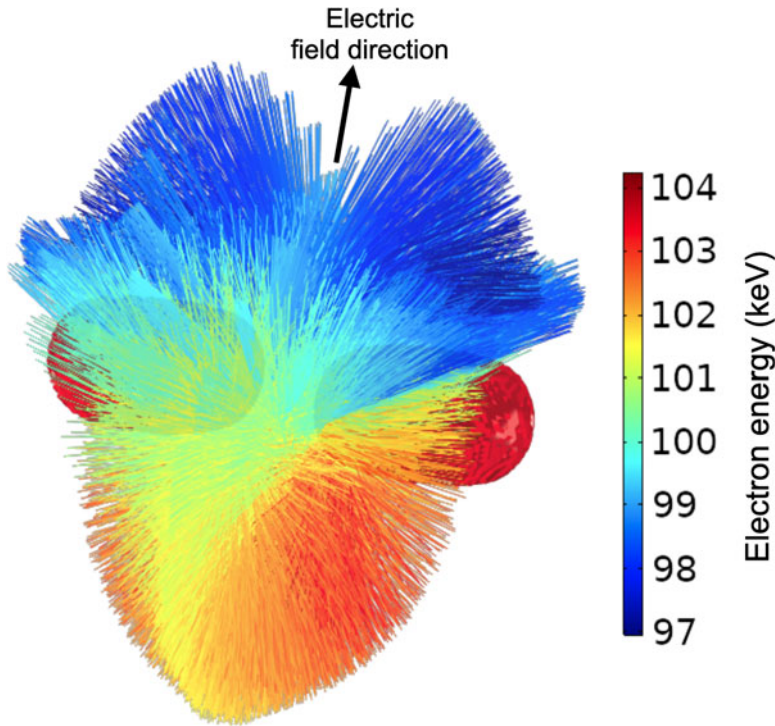


FIGURE 8. Electron trajectories between two expanding magnetic toroids (shown in dark red). The initial electron energy is 100 keV. The trajectories are traced by solving the relativistic equations of motion with the COMSOL Multiphysics package. The trajectories are represented in terms of the electron energy that is shown in the colour bar.

4.4. Betatron acceleration

The betatron mechanism accelerates charged particles spiralling about the magnetic field lines due to conservation of the magnetic moment $\mu = mv^2/2B$ in a dynamically increasing magnetic field. This effect is used and observed in many applications ranging from particle accelerators (Kerst 1940) to solar flares (Somov *et al.* 2003; Chen *et al.* 2020).

Magnetized plasmas colliding with a high, super-Alfvénic, supersonic velocity exhibit a strong transient jump of the magnetic field across the collision interface because of the plasma compression – so-called magnetic field pileup. This effect can accelerate the reconnection by compressing the magnetic field and therefore the local Alfvén velocity $V_A = B/(\mu_0\rho)^{1/2}$, where ρ is the total plasma mass density. Recent observations in the Earth’s magnetosphere revealed flux pileup by a factor of 3 to 5 (Fu *et al.* 2013; Øieroset *et al.* 2019), a factor of between 1 and 5 in the solar photosphere (Litvinenko, Chae & Park 2007), and a factor of 2 in a high-energy-density plasma (Suttle *et al.* 2018). In the above cited works it was also observed that plasma in the flux pileup region was heated.

Returning to laser-driven reconnection experiments, two-dimensional particle-in-cell simulations (Fox, Bhattacharjee & Germaschewski 2011, 2012) with plasma profiles and parameters relevant to our experiments showed pileups reaching up to a factor of 4, depending on the inflow Mach number. However, these two-dimensional simulations are relatively over-compressive because in reality the plumes simultaneously are expanding (and decompressing) in the out-of-plane direction. Recent three-dimensional simulations

obtain a smaller but finite pileup, close to a factor of 1.5–2 (Matteucci *et al.* 2018). Other two-dimensional simulations (Totorica *et al.* 2016) observed a field enhancement of a factor of 1.5–5, depending on the inflow Mach number, and decreasing to about 7% for a three-dimensional case for an inflow Mach number $M_A = V_{\text{in}}/V_A = 4$. For comparison, the inflow Mach number in our experiment was $M_A = 10$ –12.

For these reasons, we hypothesize that the electrons are accelerated in concert with the magnetic compression into the reconnection layer in the strongly driven regime. These electrons are magnetized by the strong magnetic field and therefore can stay confined to the plumes for the time scale of the interaction, rather than being promptly lost. To explain the observed energy gain dependency on the energy ($\Delta E \approx 0.5E$), a 50% field increase would be required.

5. Plasma parameters

In this section we present results of experiments justifying the choice of plasma parameters, such as density, temperature, flow speed and magnetic field, used for various numerical estimates throughout the paper.

5.1. Magnetic field and plasma bubble expansion

Much work has been published on Biermann magnetic field measurements in laser plasmas using proton radiography (Li *et al.* 2007; Petrasso *et al.* 2009; Gao *et al.* 2015; Rosenberg *et al.* 2015a,b). The quantity that is directly inferred from these measurements is not the magnetic field *per se*, but its integral, $\int B dl$, along the proton path. Incidentally, it is exactly the same quantity that determines the acceleration by the reconnection electric field – equation (4.1).

The measurements published in Petrasso *et al.* (2009) were done under conditions very similar to those in our experiment, namely using a 5 μm thick CH foil irradiated by a laser beam with an intensity of $8 \times 10^{13} \text{ W cm}^{-2}$, focused to a diameter of 850 μm . Those results reveal a toroidal magnetic field structure expanding with a velocity of $V_{\text{in}} \approx 5 \times 10^5 \text{ m s}^{-1}$, with a peak of the field integral of $\int B dz = 10 \text{ T mm}$, the values we use in our paper. Somewhat higher magnetic field and expansion velocity, 16 T mm and $7 \times 10^5 \text{ m s}^{-1}$, respectively, were inferred from measurements in Rosenberg *et al.* (2015b), but they were made at a laser intensity higher by a factor of two.

5.2. Plasma density and temperature

Plasma parameters were probed with temporally resolved Thomson scattering using a 2ω probe beam (527 nm, 50 J, 1 ns) (Follett *et al.* 2016). Scattered light from the probe beam was collected from a localized volume ($50 \times 50 \times 70 \mu\text{m}^3$) centred midway between the two drive beams. The scattering angle was 63° , yielding a scattering parameter $\alpha = 1/k\lambda_{\text{de}} = 1.2$ for typical plasma parameters (i.e. the collective regime). The collected light was scattered from electron plasma waves, which can provide information on the electron density and temperature, passed through a spectrometer with a wavelength resolution of 0.5 nm and imaged onto a streak camera with a temporal resolution of 50 ps. The scattered signal was streaked for 1 ns starting 1.5 ns after the drive beams.

To perform error analysis, we employ a Monte Carlo approach in which the extracted plasma parameters represent the mean value over 50 fits, with error bars corresponding to the standard deviation. In all cases, the electron plasma wave spectra fits assumed a Maxwellian velocity distribution.

The results depicted in figure 9 show a nearly constant electron temperature $T_e \approx 400 \text{ eV}$ over the probed time range, and a slowly increasing density that plateaus around $n_e \approx 1.5 \times 10^{19} \text{ cm}^{-3}$.

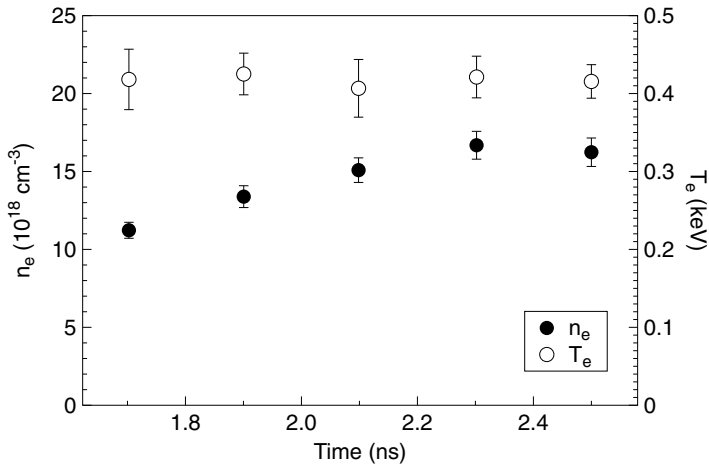


FIGURE 9. Time evolution of the plasma density n_e and electron temperature T_e .

6. Conclusions

In this series of experiments, electron energization during collision and merging of plasma plumes was studied and a positive energization in the interaction and merging of the two plumes was demonstrated. To isolate the merging as an acceleration source, the electron energy spectra obtained from two-plume collision shots are compared with the spectra from single-plume shots. It was established that even for a case of a single plume, a copious amount of energetic electrons with energies reaching hundreds of keV were present. For colliding and merging plasma plumes, electrons are additionally accelerated by several tens and up to hundreds of keV. We emphasize here that this kind of comparison of merging and ‘null’ shots, a comparison which, to our knowledge, has not previously been reported, is absolutely crucial for positively identifying the effect of merging and/or reconnection.

Our estimates and simple model simulations demonstrate that the electron energization due to the Fermi effect and/or to the electric field induced in the current sheet region is much lower than the observed gain. This observation makes us conclude that some other mechanisms are involved, for example the betatron effect in the dynamically changing magnetic field during the merging and/or reconnection. The energy gain due to the betatron effect is proportional to the particle initial energy, in agreement with the experimental signatures.

While the electron energization by the betatron effect sounds like a potentially compelling explanation, it is not inherently related to reconnection, *per se*. To better differentiate between the two mechanisms, we plan to conduct experiments with colliding parallel magnetic fields, similar to what was done in Rosenberg *et al.* (2015a). In those types of shots, the reconnection would be eliminated, but the possibility for the betatron effect still remains because of the field amplification during collision. In addition, employing spatially and temporally resolved measurements of energized electron populations (e.g. via Thomson scattering or X-ray imaging) may be able to discern further between possible energization mechanisms.

Acknowledgements

The authors acknowledge the support of the University of Rochester and the New York State Energy Research and Development Authority.

Editor Dmitri Uzdensky thanks the referees for their advice in evaluating this article.

Funding

This work was supported through LaserNetUS at the OMEGA EP facility (contract number DE-SC0020005) and by the Department of Energy National Nuclear Security Administration (award number DE-NA0003856).

Declaration of interest

The authors report no conflict of interest.

REFERENCES

- BHATTACHARJEE, A. 2004 Impulsive magnetic reconnection in the earth's magnetotail and the solar corona. *Annu. Rev. Astron. Astrophys.* **42**, 365–384.
- BIERMANN, L. 1950 *Z. Naturforsch.* **5a**, 65.
- BIRN, J., ARTEMYEV, A.V., BAKER, D.N., ECHIM, M., HOSHINO, M. & ZELENYI, L.M. 2012 Particle acceleration in the magnetotail and aurora. *Space Sci. Rev.* **173** (1), 49–102.
- BOEHLY, T.R., BROWN, T.R., CRAXTON, D.L., KECK, R.S., KNAUER, R.L., KELLY, J.P., KESSLER, J.H., KUMPAN, T.J., LOUCKS, S.A., LETZRING, S.J., MARSHALL, S.A., MCCRORY, F.J., MORSE, R.L., SEKA, S.F.B., SOURES, W.J.M. & VERDON, C.P. 1977 *Opt. Commun.* **133**, 495.
- BONNET, T., COMET, M., DENIS-PETIT, D., GOBET, F., HANNACHI, F., TARISIEN, M., VERSTEEGEN, M. & ALEONARD, M.M. 2013 Response functions of imaging plates to photons, electrons and He-4 particles. *Rev. Sci. Instrum.* **84** (10).
- BOOK, D.L. 1990 *NRL Plasma Formulary*. Naval Research Laboratory, USA.
- CHEN, B., SHEN, C., GARY, D.E., REEVES, K.K., FLEISHMAN, G.D., YU, S., GUO, F., KRUCKER, S., LIN, J., NITA, G.M. & KONG, X. 2020 Measurement of magnetic field and relativistic electrons along a solar flare current sheet. *Nature Astron.* **4**, 1140–1147.
- DONG, Q., WANG, S., LU, Q., HUANG, C., YUAN, D., X.LIU, LIN, X., WEI, H., ZHONG, J., SHI, J., JIANG, S., DING, Y., JIANG, B., DU, K., HE, X., YU, M. Y., LIU, C. S., WANG, S., TANG, Y., ZHU, J., ZHAO, G., SHENG, Z. & ZHANG, J. 2012 *Phys. Rev. Lett.* **108**, 215001.
- DRAKE, J.F., SWISDAK, M. & FERMO, R. 2012 The power-law spectra of energetic particles during multi-island magnetic reconnection. *Astrophys. J.* **763** (1), L5–6.
- FIKSEL, G., ALMAGRI, A.F., CHAPMAN, B.E., MIRNOV, V.V., REN, Y., SARFF, J.S. & TERRY, P.W. 2009 Mass-dependent ion heating during magnetic reconnection in a laboratory plasma. *Phys. Rev. Lett.* **103** (1), 145002.
- FIKSEL, G., FOX, W., BHATTACHARJEE, A., BARNAK, D.H., CHANG, P.Y., GERMASCHEWSKI, K., HU, S.X. & NILSON, P.M. 2014 Magnetic reconnection between colliding magnetized laser-produced plasma plumes. *Phys. Rev. Lett.* **113** (1), 105003.
- FOLLETT, R.K., DELETTREZ, J.A., EDGELL, D.H., HENCHEN, R.J., KATZ, J., MYATT, J.F. & FROULA, D.H. 2016 Plasma characterization using ultraviolet Thomson scattering from ion-acoustic and electron plasma waves (invited). *Rev. Sci. Instrum.* **87** (1), 11E401.
- FOX, W., BHATTACHARJEE, A. & GERMASCHEWSKI, K. 2011 Fast magnetic reconnection in laser-produced plasma bubbles. *Phys. Rev. Lett.* **106** (21), 215003.
- FOX, W., BHATTACHARJEE, A. & GERMASCHEWSKI, K. 2012 Magnetic reconnection in high-energy-density laser-produced plasmas. *Phys. Plasmas* **19** (5), 6309.
- FOX, W., FIKSEL, G., BHATTACHARJEE, A., CHANG, P.Y., GERMASCHEWSKI, K., HU, S.X. & NILSON, P.M. 2013 Filamentation instability of counterstreaming laser-driven plasmas. *Phys. Rev. Lett.* **111** (2), 225002.
- FOX, W., PARK, J., DENG, W., FIKSEL, G., SPITKOVSKY, A. & BHATTACHARJEE, A. 2017 Astrophysical particle acceleration mechanisms in colliding magnetized laser-produced plasmas. *Phys. Plasmas* **24** (9), 092901–10.

- FOX, W., PORKOLAB, M., EGEDAL, J., KATZ, N. & LE, A. 2010 Laboratory observations of electron energization and associated lower-hybrid and Trivelpiece-Gould wave turbulence during magnetic reconnection. *Phys. Plasmas* **17** (7), 072303.
- FOX, W., SCHAEFFER, D.B., ROSENBERG, M.J., FIKSEL, G., MATTEUCCI, J., PARK, H.S., BOTT, A.F.A., LEZHININ, K., BHATTACHARJEE, A., KALANTAR, D., REMINGTON, B.A., UZDENSKY, D., LI, C.K., SEGUIN, F.H. & HU, S.X. 2020 Fast magnetic reconnection in highly-extended current sheets at the national ignition facility. arXiv2003.06351.
- FU, H.S., KHOTYAINTSEV, Y.V., VAIVADS, A., RETINÒ, A. & ANDRÉ, M. 2013 Energetic electron acceleration by unsteady magnetic reconnection. *Nat. Phys.* **9** (7), 426–430.
- GALES, S. & BENTLEY, C. 2004 Image plates as x-ray detectors in plasma physics experiments. *Rev. Sci. Instrum.* **75** (10), 4001–4003.
- GAO, L., NILSON, P.M., IGUMENSHCHEV, I.V., HAINES, M.G., FROULA, D.H., BETTI, R. & MEYERHOFER, D.D. 2015 Precision mapping of laser-driven magnetic fields and their evolution in high-energy-density plasmas. *Phys. Rev. Lett.* **114** (2), 215003.
- HABARA, H., IWAWAKI, T., GONG, T., WEI, M.S., IVANCIC, S.T., THEOBALD, W., KRAULAND, C.M., ZHANG, S., FIKSEL, G. & TANAKA, K.A. 2019 A ten-inch manipulator (TIM) based fast-electron spectrometer with multiple viewing angles (OU-ESM). *Rev. Sci. Instrum.* **90** (6), 063501–6.
- HOSHINO, M. 2012 Stochastic particle acceleration in multiple magnetic islands during reconnection. *Phys. Rev. Lett.* **108** (13), 135003.
- HSU, S.C., CARTER, T.A., FIKSEL, G., JI, H., KULSRUD, R.M. & YAMADA, M. 2001 Experimental study of ion heating and acceleration during magnetic reconnection. *Phys. Plasmas* **8** (5), 1916–1928.
- HUNTINGTON, C.M., *et al.* 2015 Observation of magnetic field generation via the Weibel instability in interpenetrating plasma flows. *Nat. Phys.* **11** (2), 173–176.
- KERST, D.W. 1940 Acceleration of electrons by magnetic induction. *Phys. Rev.* **58** (9), 841.
- KRUEER, W.L. 1988 *The Physics of Laser Plasma Interaction*. Addison-Wesley.
- KUGLAND, N.L., KUGLAND, N.L., RYUTOV, D.D., RYUTOV, D.D., PLECHATY, C., PLECHATY, C., ROSS, J.S., ROSS, J.S., PARK, H.S. & PARK, H.S. 2012 Invited article: relation between electric and magnetic field structures and their proton-beam images. *Rev. Sci. Instrum.* **83** (10), 101301.
- LANDAU, L.D. & LIFSHITZ, E.M. 1981 *Mechanics*. Reed Educational and Professional Publishing Ltd.
- LI, C.K., SEGUIN, F.H., FRENJE, J.A., RYGG, J.R., PETRASSO, R.D., TOWN, R.P.J., LANDEN, O.L., KNAUER, J.P. & SMALYUK, V.A. 2007 Observation of megagauss-field topology changes due to magnetic reconnection in laser-produced plasmas. *Phys. Rev. Lett.* **99** (5), 55001.
- LIN, J. & FORBES, T.G. 2000 Effects of reconnection on the coronal mass ejection process. *J. Geophys. Res.: Space Phys.* **105** (A2), 2375–2392.
- LITVINENKO, Y.E., CHAE, J. & PARK, S.-Y. 2007 Flux pile-up magnetic reconnection in the solar photosphere. *Astrophys. J.* **662** (2), 1302–1308.
- MATTEUCCI, J., FOX, W., BHATTACHARJEE, A., SCHAEFFER, D.B., MOISSARD, C., GERMASCHESKI, K., FIKSEL, G. & HU, S.X. 2018 Biermann-battery-mediated magnetic reconnection in 3D colliding plasmas. *Phys. Rev. Lett.* **121** (9), 095001.
- MIYAHARA, J., TAKHASHI, K., AMEMIYA, Y., KAMIYA, N. & SATOW, Y. 1986 A new type of X-ray area detector utilizing laser stimulated luminescence. *Nucl. Instrum. Meth. Phys. Res.* **246** (1), 572–578.
- NILSON, P.M., WILLINGALE, L., KALUZA, M.C., KAMPERIDIS, C., MINARDI, S., WEI, M.S., FERNANDES, P., NOTLEY, M., BANDYOPADHYAY, S., SHERLOCK, M., KINGHAM, R.J., TATARAKIS, M., NAJMUDIN, Z., ROZMUS, W., EVANS, R.G., HAINES, M.G., DANGOR, A.E. & KRUSHELNICK, K. 2006 Magnetic reconnection and plasma dynamics in two-beam laser-solid interactions. *Phys. Rev. Lett.* **97** (2), 255001.
- NILSON, P.M., WILLINGALE, L., KALUZA, M.C., KAMPERIDIS, C., MINARDI, S., WEI, M.S., FERNANDES, P., NOTLEY, M., BANDYOPADHYAY, S., SHERLOCK, M., KINGHAM, R.J., TATARAKIS, M., NAJMUDIN, Z., ROZMUS, W., EVANS, R.G., HAINES, M.G., DANGOR, A.E. & KRUSHELNICK, K. 2008 Bidirectional jet formation during driven magnetic reconnection in two-beam laser-plasma interactions. *Phys. Plasmas* **15** (9), 2701.

- NIST 2021 Stopping power and range tables for electrons. Available at: <https://physics.nist.gov/physrefdata/star/text/estar.html>.
- ØIEROSET, M., *et al.* 2019 Reconnection with magnetic flux pileup at the interface of converging jets at the magnetopause. *Geophys. Res. Lett.* **46** (4), 1937–1946.
- PARKER, E.N. 1963 The solar-flare phenomenon and the theory of reconnection and annihilation of magnetic fields. *Astrophys. J. Suppl.* **8**, 177.
- PETRASSO, R.D., LI, C.K., SEGUIN, F.H., RYGG, J.R., FRENJE, J.A., BETTI, R., KNAUER, J.P., MEYERHOFER, D.D., AMENDT, P.A., FROULA, D.H., LANDEN, O.L., PATEL, P.K., ROSS, J.S. & TOWN, R.P.J. 2009 Lorentz mapping of magnetic fields in hot dense plasmas. *Phys. Rev. Lett.* **103** (8), 085001.
- PRIEST, E. & FORBES, T. 2000 *Magnetic Reconnection*. Cambridge University Press.
- REGAN, S.P., BRADLEY, D.K., CHIROKIKH, A.V., CRAXTON, R.S., MEYERHOFER, D.D., SEKA, W., SHORT, R.W., SIMON, A., TOWN, R.P.J., YAAKOBI, B., CARROLL III, J.J. & DRAKE, R.P. 1999 Laser-plasma interactions in long-scale-length plasmas under direct-drive national ignition facility conditions. *Phys. Plasmas* **6** (5), 2072–2080.
- ROSENBERG, M.J., LI, C.K., FOX, W., IGUMENSHCHEV, I., SEGUIN, F.H., TOWN, R.P.J., FRENJE, J.A., STOECKL, C., GLEBOV, V. & PETRASSO, R.D. 2015a First experiments probing the collision of parallel magnetic fields using laser-produced plasmas. *Phys. Plasmas* **22** (4), 042703.
- ROSENBERG, M.J., LI, C.K., FOX, W., ZYLSTRA, A.B., STOECKL, C., SEGUIN, F.H., FRENJE, J.A. & PETRASSO, R.D. 2015b Slowing of magnetic reconnection concurrent with weakening plasma inflows and increasing collisionality in strongly driven laser-plasma experiments. *Phys. Rev. Lett.* **114** (20), 205004.
- ROSENBERG, M.J., SOLODOV, A.A., SEKA, W., FOLLETT, R.K., MYATT, J.F., MAXIMOV, A.V., REN, C., CAO, S., MICHEL, P., HOHENBERGER, M., PALASTRO, J.P., GOYON, C., CHAPMAN, T., RALPH, J.E., MOODY, J.D., SCOTT, R.H.H., GLIZE, K. & REGAN, S.P. 2020 Stimulated Raman scattering mechanisms and scaling behavior in planar direct-drive experiments at the national ignition facility. *Phys. Plasmas* **27** (4), 042705.
- SCHAEFFER, D.B., FOX, W., HABERBERGER, D., FIKSEL, G., BHATTACHARJEE, A., BARNAK, D.H., HU, S.X. & GERMASCHESKI, K. 2017 Generation and evolution of high-Mach-number laser-driven magnetized collisionless shocks in the laboratory. *Phys. Rev. Lett.* **119** (2), 025001–6.
- SOLODOV, A.A., ROSENBERG, M.J., SEKA, W., MYATT, J.F., HOHENBERGER, M., EPSTEIN, R., STOECKL, C., SHORT, R.W., REGAN, S.P., MICHEL, P., CHAPMAN, T., FOLLETT, R.K., PALASTRO, J.P., FROULA, D.H., RADHA, P.B., MOODY, J.D. & GONCHAROV, V.N. 2020 Hot-electron generation at direct-drive ignition-relevant plasma conditions at the national ignition facility. *Phys. Plasmas* **27** (5), 052706.
- SOMOV, B.V., ORESHINA, A.V., ORESHINA, I.V. & SHAKURA, N.I. 2003 Flares in accretion disk coronae. *Adv. Space Res.* **32** (6), 1087–1096.
- SUTTLE, L.G., HARE, J.D., LEBEDEV, S.V., CIARDI, A., LOUREIRO, N.F., BURDIAC, G.C., CHITTENDEN, J.P., CLAYSON, T., HALLIDAY, J.W.D., NIASSE, N., RUSSELL, D., SUZUKI-VIDAL, F., TUBMAN, E., LANE, T., MA, J., ROBINSON, T., SMITH, R.A. & STUART, N. 2018 Ion heating and magnetic flux pile-up in a magnetic reconnection experiment with super-Alfvénic plasma inflows. *Phys. Plasmas* **25** (4), 042108.
- TANABE, H., YAMADA, T., WATANABE, T., GI, K., INOMOTO, M., IMAZAWA, R., GRYAZNEVICH, M., MICHAEL, C., CROWLEY, B., CONWAY, N.J., SCANNELL, R., HARRISON, J., FITZGERALD, I., MEAKINS, A., HAWKES, N., MCCLEMENTS, K.G., O’GORMAN, T., CHENG, C.Z. & ONO, Y. 2017 Recent progress of magnetic reconnection research in the MAST spherical tokamak. *Phys. Plasmas* **24** (5), 056108.
- TOTORICA, S.R., ABEL, T. & FIUZA, F. 2016 Nonthermal electron energization from magnetic reconnection in laser-driven plasmas. *Phys. Rev. Lett.* **116** (9), 095003–5.
- TOTORICA, S.R., ABEL, T. & FIUZA, F. 2017 Particle acceleration in laser-driven magnetic reconnection. *Phys. Plasmas* **24** (4), 041408–13.
- WAXER, L.J., MAYWAR, D.N., KESSLER, T.J., KRUSCHWITZ, B.E., LOUCKS, S.J., MCCRORY, R.L., MEYERHOFER, D.D., MORSE, S.F.B., STOECKL, C. & ZUEGEL, J.D. 2005 High-energy petawatt capability of omega laser. *Opt. Photonics News* **16**, 30.

- YAMADA, M., LEVINTON, F.M., POMPHREY, N., BUDNY, R., MANICKAM, J. & NAGAYAMA, R. 1994 Investigation of magnetic reconnection during a sawtooth crash in a high-temperature tokamak plasma. *Phys. Plasmas* **1**, 3269.
- YAMASAKI, K., INOUE, S., KAMIO, S., WATANABE, T.G., USHIKI, T., GUO, X., SUGAWARA, T., MATSUYAMA, K., KAWAKAMI, N., YAMADA, T., INOMOTO, M. & ONO, Y. 2015 Laboratory study of diffusion region with electron energization during high guide field reconnection. *Phys. Plasmas* **22** (1), 101202.
- ZHONG, J., LI, Y., WANG, X., WANG, J., DONG, Q., XIAO, C., WANG, S., LIU, X., ZHANG, L., AN, L., WANG, F., ZHU, J., GU, Y., HE, X., ZHAO, G. & ZHANG, J. 2010 Modelling loop-top X-ray source and reconnection outflows in solar flares with intense lasers. *Nat. Phys.* **6**, 984–987.
- ZHONG, J.Y., *et al.* 2016 Relativistic electrons produced by reconnecting electric fields in a laser-driven bench-top solar flare. *Astrophys. J. Suppl. Ser.* **225** (2), 30.